ARTICLE NO. 79-4058

Time-Variant Aerodynamics of Oscillating Airfoil Surfaces in a Supersonic Flowfield

Sanford Fleeter* and Ronald E. Riffel†
Detroit Diesel Allison, Divison of General Motors, Indianapolis, Ind.

The results of an experimental study of the time-variant aerodynamics associated with harmonically oscillating single airfoil surfaces in a supersonic flowfield are presented. Six single airfoil configurations were investigated: a flat plate, wedge, flat plate-convex corner, wedge-convex corner, MCA suction surface, and MCA pressure surface. The basic time-variant aerodynamic data obtained for each of these configurations included the chordwise distribution of the unsteady pressure magnitude (expressed as an unsteady pressure coefficient) and its phase lag as referenced to the airfoil motion, with Mach number as parameter. All of the data obtained are correlated with a low reduced frequency prediction which includes the effects of airfoil camber and thickness distribution.

Nomenclature

C = airfoil chord
C_p = unsteady pressure coefficiency
k = reduced frequency, $k = \omega C/2U$
M = Mach number
N = total number of dynamic data points
P = unsteady pressure amplitude
P_s = inlet static pressure
r = lag number
R_a = digitizing rate
R_{xr} = normalized autocorrelation function
R_{xyr} = normalized cross-correlation function
U = inlet velocity
α = torsional amplitude of oscillation
γ = ratio of specific heats
θ = phase
ω = frequency of oscillation

Introduction

THE prediction of the time-variant pressure on transonic/supersonic fan or compressor blade rows has become a problem of growing importance. The generally used flow model considers inviscid flow past harmonically oscillating two-dimensional flat plate airfoil cascades. Such a simplified model is made necessary by the extremely complex nature of the relevant unsteady aerodynamic phenomena. Recently, a number of solutions involving various mathematical techniques have been and continue to be developed, as noted and discussed in Ref. 1.

To extend this model to more realistic airfoil configurations, it is necessary to develop a physical understanding of the fundamental unsteady aerodynamics. Toward this end, analyses of single cambered and/or thick airfoils harmonically oscillating in a supersonic stream are appearing in the literature.[1-4] Such analyses retain the fundamental physics but eliminate the further complication of the mutual aerodynamic interference of the blading.

However, as has been noted in various places, Refs. 5 and 6 for example, unsteady aerodynamic data are necessary to further the understanding of the basic physics and the development of the various theoretical approaches. The present work involves an experimental investigation of the time-variant aerodynamics associated with harmonically oscillating two-dimensional flat plate, wedge, flat plate-convex corner, wedge-convex corner, and MCA cambered airfoil surfaces in a supersonic flowfield.

Airfoils and Dynamic Instrumentation

Two double-trunnion steel airfoils, characterized by a 3.0 in. (7.62 cm) span, a 2.5 in. (6.35 cm) chord, and a torsional axis located at midchord were used in the investigation. The classical airfoil consisted of a flat suction surface and a triangular pressure surface, schematically depicted in Fig. 1. The second airfoil, schematically depicted in Fig. 2 with coordinates presented in Table 1, was modeled from the multiple-circular-arc (MCA) tip section of an advanced design fan blade.

Each of the airfoils was machined to permit the chordwise imbedding of miniature Kulite LQ series dynamic pressure transducers, staggered across the span such that the airfoil surface contours were preserved. The chordwise transducer locations, schematically indicated in Figs. 1 and 2, are presented in Table 2.

The single airfoil mounting arrangement in the supersonic wind-tunnel test section is shown schematically in Fig. 3. Strain gages, mounted on the spring bars, exhibit excellent sensitivity to the torsional movement of the airfoils and allow the measured strain gage signals to be converted to rotational amplitudes. The double-trunnion airfoils and spring bar assemblies are mounted in plexiglas wind-tunnel test section walls, thereby permitting Schlieren flow visualization. Driving arms are attached to the airfoil trunnions which are driven by means of electromagnets, as described in detail in Ref. 7.

Experimental Technique

The Detroit Diesel Allison (DDA) supersonic wind tunnel was designed as part of a continuous flow, nonreturn system.

Received April 19, 1978; revision received Nov. 6, 1978.

Index categories: Nonsteady Aerodynamics; Supersonic and Hypersonic Flow.

*Supervisor, Cascade & Flow Systems Research; presently Associate Professor, School of Mechanical Engineering, Purdue University, West Lafayette, Ind. Member AIAA.

†Senior Research Engineer. Member AIAA.

Table 1 MCA airfoil coordinates

$X_{suction}$ in. (cm)	$Y_{suction}$, in. (cm)	$X_{pressure}$, in. (cm)	$Y_{pressure}$, in. (cm)
0.0000 (0.0000)	0.0215 (0.0546)	0.0000 (0.0000)	0.0178 (0.0452)
0.1303 (0.3310)	0.0246 (0.0625)	0.1574 (0.3993)	0.0010 (0.0025)
0.2882 (0.7320)	0.0241 (0.0612)	0.3147 (0.7993)	−0.0133 (−0.0338)
0.4459 (1.1326)	0.0240 (0.0610)	0.4724 (1.1999)	−0.0250 (−0.0635)
0.6036 (1.5331)	0.0242 (0.0615)	0.6302 (1.6007)	−0.0343 (−0.0871)
0.7612 (1.9334)	0.0247 (0.0627)	0.7882 (2.0020)	−0.0410 (−0.1041)
0.9188 (2.3338)	0.0256 (0.0650)	0.9463 (2.4036)	−0.0453 (−0.1151)
1.0763 (2.7338)	0.0269 (0.0683)	1.1045 (2.8054)	−0.0470 (−0.1194)
1.2337 (3.1336)	0.0281 (0.0714)	1.2627 (3.2073)	−0.0462 (−0.1173)
1.3912 (3.5336)	0.0304 (0.0772)	1.4208 (3.6088)	−0.0429 (−0.1090)
1.5487 (3.9337)	0.0327 (0.0831)	1.5788 (4.0102)	−0.0370 (−0.0940)
1.7062 (4.3337)	0.0353 (0.0897)	1.7368 (4.4115)	−0.0287 (−0.0729)
1.8638 (4.7341)	0.0383 (0.0973)	1.8945 (4.8120)	−0.0178 (−0.0452)
2.0219 (5.1356)	0.0406 (0.1031)	2.0516 (5.2111)	−0.0062 (−0.0157)
2.1802 (5.5377)	0.0394 (0.1001)	2.2089 (5.6106)	0.0039 (0.0099)
2.3383 (5.9393)	0.0344 (0.0874)	2.3664 (6.0107)	0.0124 (0.0315)
2.4962 (6.3403)	0.0256 (0.0650)	2.4965 (6.3411)	0.0220 (0.0559)

Table 2 Percent chord locations of dynamic pressure transducers

Classical airfoil, % chord		MCA airfoil, % chord	
Suction	Suction	Suction	Suction
22.5	13.5	14.0	14.5
45.0	25.0	34.5	36.0
63.0	40.0	54.5	55.0
81.0	61.9	65.0	65.0
95.0	73.5	75.5	74.5
	85.5	87.0	85.0

Up to 10 lbm/s of filtered, dried, and temperature-controlled air may be used. The test section exit is evacuated by steam ejectors which can maintain an exit pressure of 6 lbf/in.^{2} absolute at the design flow rate. In this facility, the entrance flow to the test section is generated by fixed nozzle blocks yielding a Mach number of 1.50. The orientation of a wedge with respect to this nozzle exit flow specifies the test section Mach number, i.e., the shock or expansion wave generated by the wedge determines the test section inlet conditions.

The two surfaces of a single airfoil harmonically oscillating in a supersonic flowfield are independent of one another. Hence, in this single airfoil experimental study, the time-variant aerodynamics of six distinct isolated airfoil surface configurations could be determined—four for the classical single airfoil and two for the MCA airfoil—as indicated in Fig. 4. This was accomplished by appropriate choices for the alignment of the supersonic inlet flowfield with respect to the particular airfoil surfaces, i.e., setting the various airfoil surfaces parallel to the upstream wedge.

First, consider the unsteady phenomena on the flat suction surface of the classical airfoil. With the inlet flow aligned with this surface, it acts as an oscillating flat plate (configuration 1). With the inlet flow aligned with the pressure surface, the flat suction surface serves as an oscillating wedge (configuration 2).

Next, consider the phenomena on the triangular pressure surface. With the inlet flow aligned with this pressure surface, it served as an oscillating flat plate-convex corner (configuration 3). The alignment of the inlet flow with the suction surface results in this pressure surface acting as an oscillating wedge-convex corner (configuration 4).

The MCA airfoil did not permit all of the flexibility of the previously described classical airfoil. This was because it was

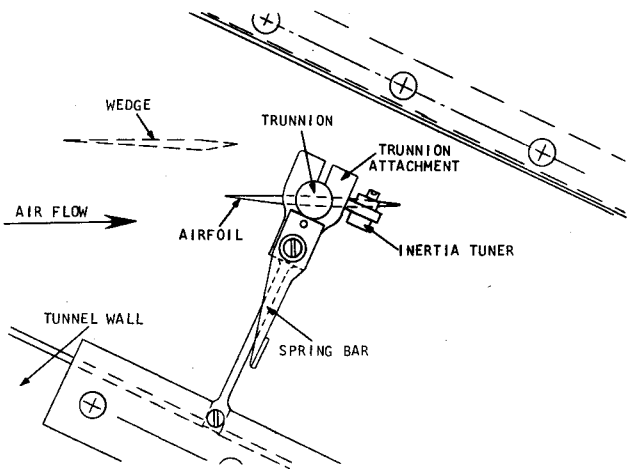

Fig. 3 Schematic of airfoil-spring bar mounting arrangement.

Fig. 1 Classical airfoil profile.

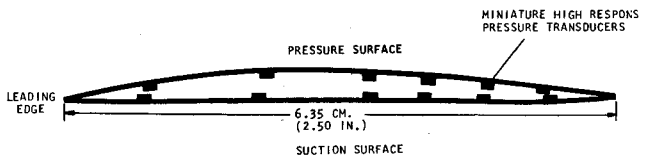

Fig. 2 Multiple-circular-arc airfoil profile.

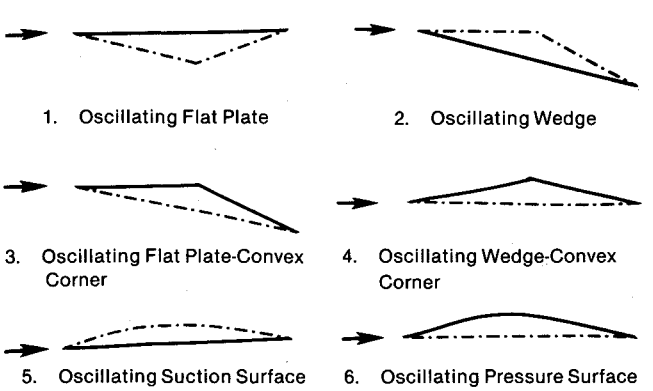

Fig. 4 Single airfoil configurations.

only possible to accurately align the inlet flow with the relatively flat leading edge portion of the suction surface, i.e., the front portion (5-40% chord) of the suction surface was flat thereby permitting accurate alignment with the wedge. It should be noted that a precompression region exists at the leading edge of this suction surface. The relatively high camber pressure surface precluded such an alignment. Hence, the inlet flowfield was always aligned with the flat region of the suction surface of the MCA airfoil. This permitted the experimental determination of the time-variant aerodynamics of two cambered airfoil profiles: the MCA airfoil's pressure surface and suction surface (configurations 5 and 6).

Dynamic Data Acquisition and Analysis

With the tunnel in operation and the flowfield properly established, as determined by sidewall static pressure taps and Schlieren flow visualization, the torsion mode drive system was made operational. This resulted in controlled harmonic oscillations of the airfoil at the prescribed frequency. The resulting time-variant spring bar mounted strain gage and airfoil surface pressure transducer signals were digitized at rates to 100,000 points/s by a 16-channel analog-digital converter and mutiplexer system and stored on a magnetic disk. These digitized data were analyzed on-line to determine the fundamental aerodynamic characteristics of the unsteady phenomena. The parameters of interest are the amplitude of the airfoil motion and the pressure disturbance, the frequency, and the phase difference between the unsteady pressures and the airfoil motion as characterized by the strain gage signal; that is, the aerodynamic phase lag data are referenced to the motion of the airfoil.

The amplitudes of the airfoil motion and the pressure disturbance are determined by fitting a second-order, least-square function to the data, differentiating it, and evaluating the maximum. The pressure disturbance amplitude is then nondimensionalized into an unsteady pressure coefficient C_p defined as:

$$C_p = p/\tfrac{1}{2}\rho U^2\alpha = p/\tfrac{1}{2}\gamma M^2 p_s\alpha \tag{1}$$

where p is the measured unsteady pressure amplitude, ρ is the fluid density, U is the inlet velocity, γ is the ratio of specific heats, p_s is the inlet static pressure, and α is the torsional amplitude of oscillation.

The frequency of the time-dependent data is determined through the autocorrelation function. This function describes the dependence on the values of the data at one time, X_i, on the values at another time, X_{i+r}. The normalized autocorrelation function, R_{xr}, is defined in series form as:

$$R_{xr} = \frac{1}{N-r}\sum_{i=1}^{N-r} X_i X_{i+r} \Big/ \frac{1}{N}\sum_{i=1}^{N} X_i X_i \quad r=0,1,2\ldots m \tag{2}$$

where X_i is $X(i\Delta t)$, r is the lag number, N is the total number of dynamic data points, and m is the number of lags.

The lag time Δt is inversely proportional to the rate at which the data are digitized. A typical autocorrelogram of the digitized data exhibits the features of a sine wave plus random noise. A second-order, least-square function is fit to the data in the second positive peak of the autocorrelogram. The inverse of the time at which this least-square function is a maximum is equal to the frequency f of the time-dependent data.

The phase difference of the pressure disturbance along the airfoil chord in relation to the airfoil motion is calculated through the cross-correlation function. This function for two sets of data, X_i, Y_i, describes the dependence of the values of one set of data on the other. The normalized cross-correlation function, R_{xyr}, is defined as:

$$R_{xyr} = \frac{1}{N-r}\sum_{i=1}^{N-r} X_i Y_{i+r} \Big/ \frac{1}{N}\sum_{i=1}^{N} X_i Y_i \quad r=-m,\ldots -1,0,1\ldots \tag{3}$$

where the variables are defined analogous to those in Eq. (2).

As in the frequency calculation, a second-order, least-square function is fit to the data in the first positive peak of the cross correlogram. The time, t_p, at which this least-square function is a maximum is determined analytically. The phase difference, in degrees, is calculated as

$$\theta_p = t_p \; f \; 360 \tag{4}$$

where f is the frequency calculated for the airfoil motion from the strain gage data utilizing Eq. (2).

Two sources of phase-relation discrepancy are inherent in the electronic data acquisition system and correlation computation. The analog/digital (A/D) converter-multiplexer unit does not permit data to be digitized simultaneously on all channels. Consequently, an inherent phase shift is introduced into the physical data when the cross-correlation function operates on the raw digitized data. This phase shift for the sinusoidal data in this experiment is directly proportional to the "cut rate" of the multiplexer as

$$\theta_s = f_x(K_y - K_x)360/R_a \tag{5}$$

where θ_s is the A/D phase shift inherent in the computation between channels K_y and K_x, representing the respective data, Y_i and X_i. The frequency, f_x, corresponds to the disturbance in channel K_x, and R_a is the rate at which the data were being digitized.

Prior to acquiring data, the electronic data acquisition system is calibrated for phase shift, θ_a, using the A/D converter and the computation described in the foregoing. Therefore, the phase difference of the pressure disturbance along the airfoil surface in relation to the airfoil motion is:

$$\theta_{xy} = \theta_p - \theta_s - \theta_a \tag{6}$$

Data-Theory Correlation

The value of the reduced frequency k ($k=\omega C/2U$) for these single airfoil tests is 0.14. As this value is relatively low, it is appropriate to correlate these dynamic data with Miles' analytical second-order results for a slowly oscillating, cambered, isolated airfoil in a supersonic flowfield per Ref. 8. This low reduced frequency analysis is also used to obtain the flat plate predictions.

Figures 5 and 6 present the aerodynamic phase lag and unsteady pressure coefficient experimental results and the low reduced frequency flat plate analytical predictions as a function of percent airfoil chord with Mach number as parameter for configuration 1—flow past an oscillating flat plate. As can be clearly seen, the aerodynamic phase lag data correlate extremely well with the prediction, with an increased

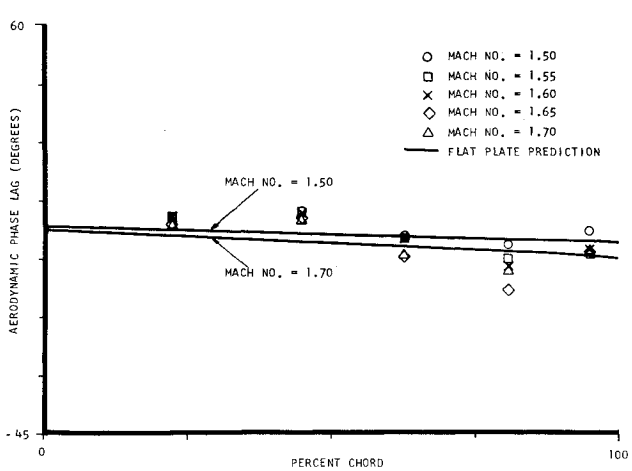

Fig. 5 Aerodynamic phase lag as a function of airfoil chord for an oscillating flat plate (configuration 1).

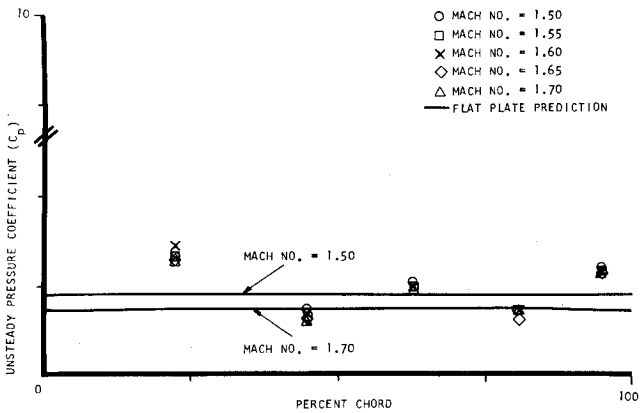

Fig. 6 Unsteady pressure coefficient as a function of airfoil chord for an oscillating flat plate (configuration 1).

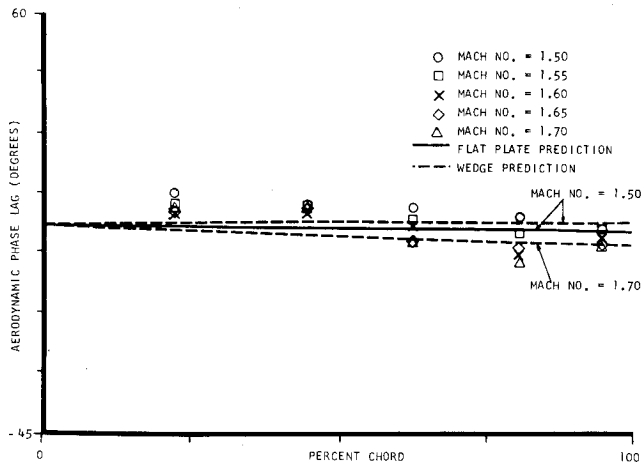

Fig. 7 Aerodynamic phase lag as a function of airfoil chord for an oscillating wedge (configuration 2).

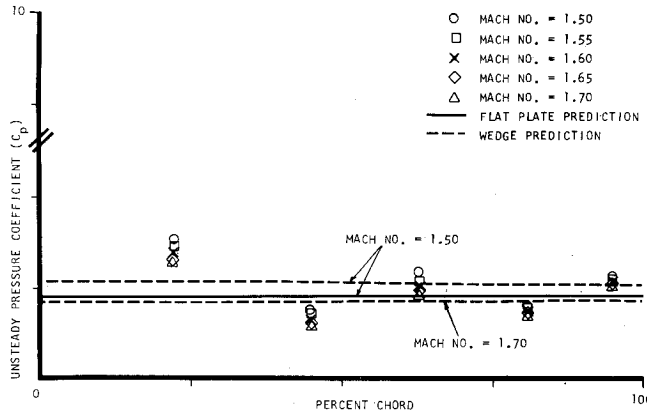

Fig. 8 Unsteady pressure coefficient as a function of airfoil chord for an oscillating wedge (configuration 2).

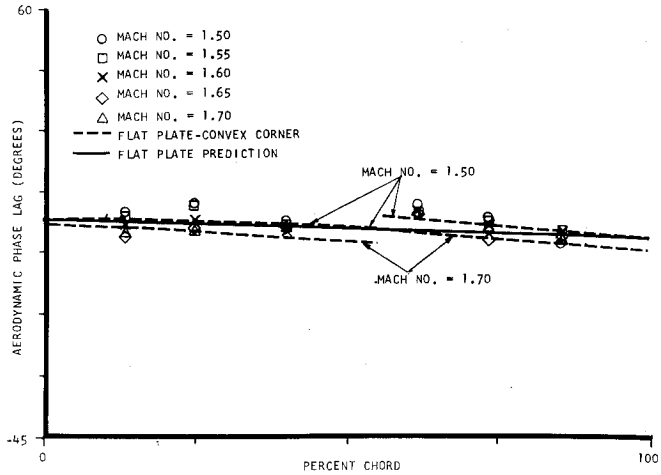

Fig. 9 Aerodynamic phase lag as a function of airfoil chord for an oscillating flat plate-convex corner (configuration 3).

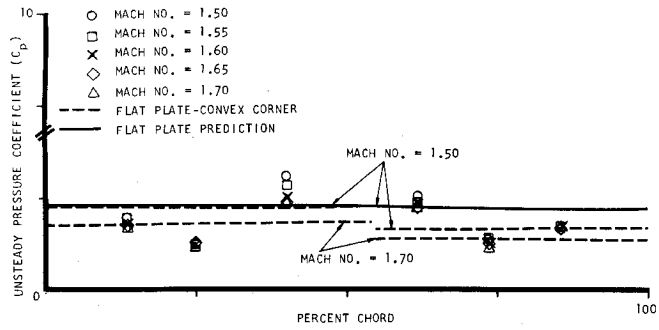

Fig. 10 Unsteady pressure coefficient as a function of airfoil chord for an oscillating flat plate-convex corner (configuration 3).

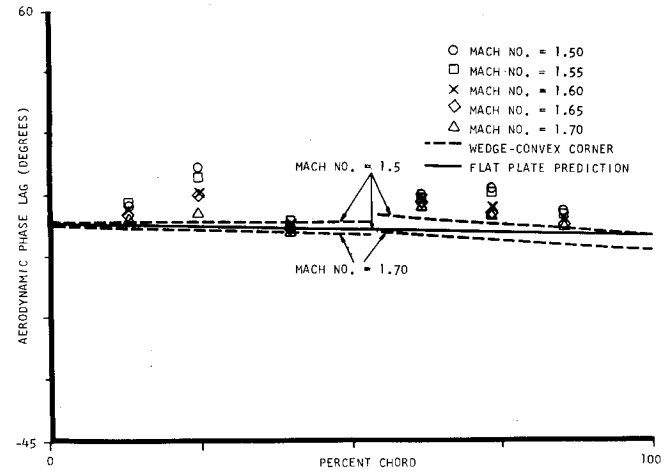

Fig. 11 Aerodynamic phase lag as a function of airfoil chord for an oscillating wedge-convex corner (configuration 4).

Mach number resulting in a decreased phase lag. The unsteady pressure coefficient correlation (Fig. 6) is also quite good, although the data appear to oscillate along the chord around the prediction.

Figures 7 and 8 show the complex unsteady pressure data for the oscillating wedge, as a funcion of airfoil chord with Mach number as parameter, together with the low reduced frequency predictions for a flat plate and for configuration 2—flow past an oscillating wedge.

As indicated, the phase lag and unsteady pressure coefficient data correlation with the wedge prediction is excellent; whereas, the correlation with the flat plate prediction is not quite as good, as anticipated. As for configuration 1—the oscillating flat plate—the unsteady pressure coefficient data appear to oscillate around the prediction along the airfoil chord.

Figures 9-12 present the aerodynamic phase lag and unsteady pressure coefficient experimental data as a function of airfoil chord with Mach number as parameter for configurations 3 and 4. These configurations correspond to flow past an oscillating flat plate-convex corner and wedge-convex corner, respectively. Also presented in these figures are the corresponding cambered airfoil profile low reduced frequency predictions as well as those for the flat plate. The

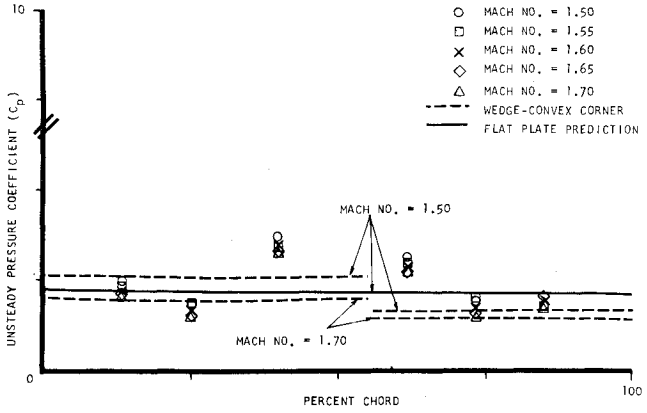

Fig. 12 Unsteady pressure coefficient as a function of airfoil chord for an oscillating wedge-convex corner (configuration 4).

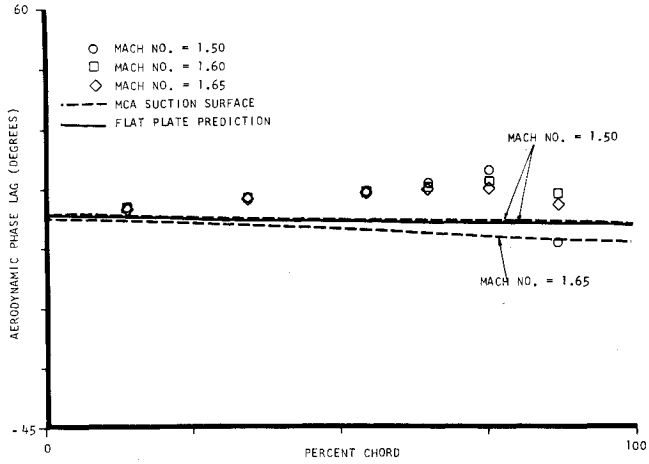

Fig. 13 Aerodynamic phase lag as a function of airfoil chord for an oscillating MCA suction surface (configuration 5).

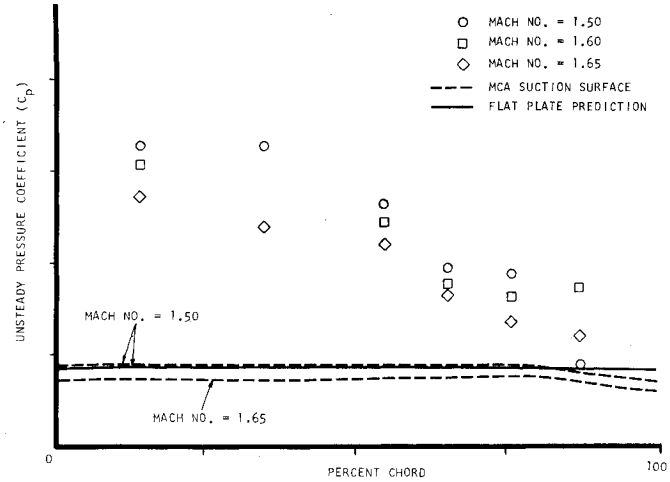

Fig. 14 Unsteady pressure coefficient as a function of airfoil chord for an oscillating MCA suction surface (configuration 5).

aerodynamic phase lag data correlate very well with the corresponding predictions and not as well with the flat plate predictions, Figs. 9 and 11. It should be noted that the front portion of configuration 3 is nearly a flat plate; hence, the profile and flat plate predictions are almost identical.

The unsteady pressure coefficient data for the flat plate-convex corner, configuration 3, exhibit these same correlation characteristics, with the data still oscillating along the chord (Fig. 10). The wedge portion of the wedge-convex corner

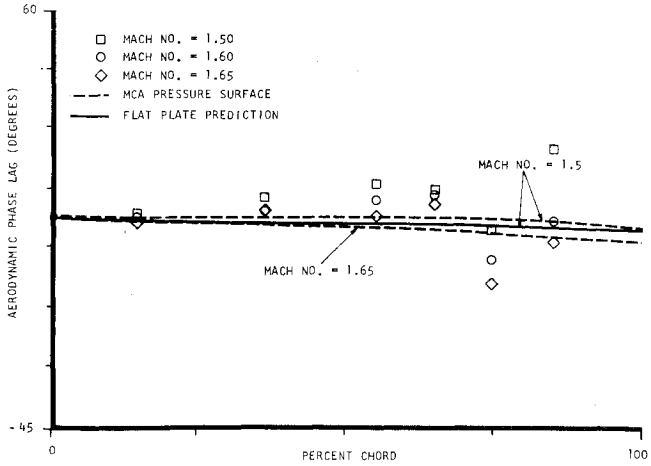

Fig. 15 Aerodynamic phase lag as a function of airfoil chord for an oscillating MCA pressure surface (configuration 6).

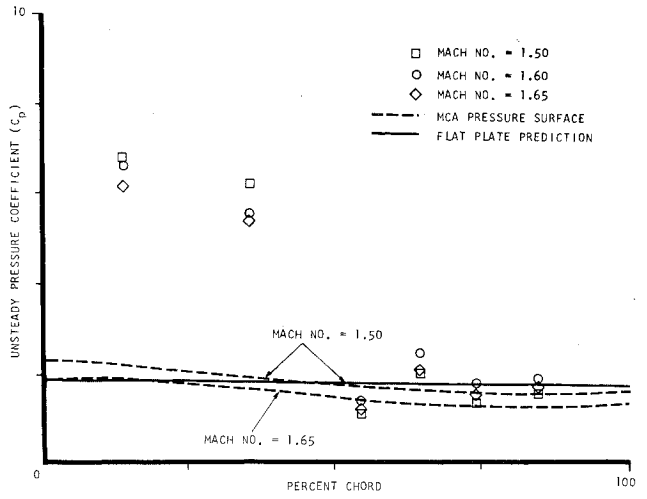

Fig. 16 Unsteady pressure coefficient as a function of airfoil chord for an oscillating MCA pressure surface (configuration 6).

unsteady pressure coefficient data correlate reasonably well with the corresponding wedge profile prediction. However, past the convex corner, these data correlate somewhat better with the flat plate prediction than with the convex corner prediction, Fig. 12. These pressure coefficient data also exhibit a tendency to oscillate along the chord.

Figures 13 and 14 present the MCA airfoil suction surface (configuration 5) complex unsteady pressure data correlation with the cambered airfoil and the flat plate predictions. As indicated, the small airfoil camber results in small differences between the flat plate and the cambered surface predictions. The trend of the data is in agreement with that of the analysis, i.e., increased Mach number yields decreased values of the aerodynamic phase lag and the unsteady pressure coefficient. However, the data show a somewhat greater phase lag than that predicted and a much increased pressure coefficient, particularly over the front 55% of the airfoil chord.

Figures 15 and 16 present the aerodynamic phase lag and unsteady pressure coefficient data with Mach number as parameter for the pressure surface of the oscillating MCA airfoil (configuration 6). As previously noted, the inlet flowfield was always aligned with the airfoil suction surface. The cambered airfoil predictions differ from those of the flat plate, as indicated. The phase lag data appear to be in relatively good agreement with the cambered airfoil predictions, with an increase in the Mach number yielding a decreased phase lag. The pressure coefficient data correlate reasonably well over the back half of the airfoil but not the

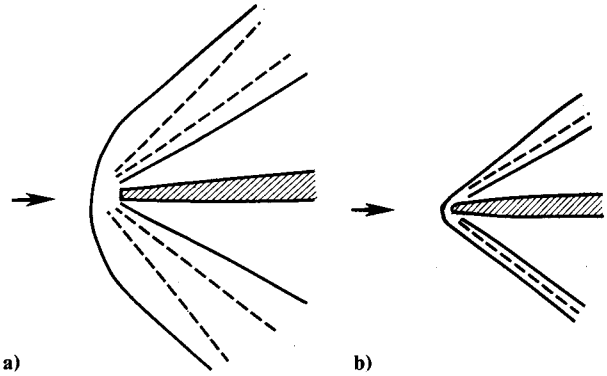

Fig. 17 Schematic of leading edge regions of a) classical diamond-back and b) MCA airfoils.

front. However, the overall trends of the data agree with the prediction, i.e., increased Mach number results in decreased values of the pressure coefficient. Also, it can be seen that the general shape of the data simulate, to some extent, that of the cambered prediction.

The question quickly arises as to why there is such excellent data-theory correlation for the classical airfoil (configurations 1-4) and not for the MCA airfoil (configurations 5 and 6). This is of particular interest over the front portion of the MCA suction surface where the surface is nearly flat, and yet there is large difference between the prediction and the unsteady pressure coefficient data (Fig. 14). One fundamental difference is that of the airfoil leading edges. The classical airfoil leading edge is blunt, whereas the MCA airfoil has a leading edge radius. Also, the MCA airfoil has some precompression on the leading edge region of the suction surface, as presented in Table 1. Besides affecting the bow waves and the initial boundary-layer characteristics, this meant that the inlet flow could be precisely aligned with the flat leading edges of both surfaces of the classical airfoil. However, for the MCA airfoil, the inlet flowfield was aligned with the flat portion of the suction surface immediately downstream of the leading edge precompression and not with the leading edge. These dissimilarities result in bow wave differences visible with the Schlieren flow visualization: the classical airfoil exhibited a relatively wide bow expansion fan, whereas the MCA one had a very narrow fan, as depicted in Fig. 17. It should be noted that computer codes are available which could be used to theoretically investigate the inviscid effects of leading edge bluntness.

Summary and Conclusions

The results of an experimental investigation of six different harmonically oscillating airfoil surfaces in a supersonic flowfield have been presented. The fundamental data obtained included the aerodynamic phase lag and the unsteady pressure coefficient as a function of airfoil chord over a range of inlet Mach number values. These data were correlated with a low reduced frequency prediction which included the effects of camber and thickness.

The data obtained for the flat plate, wedge, flat plate-convex corner, and wedge-convex corner airfoil surface configurations exhibited excellent correlation with the appropriate predictions, thereby clearly indicating the validity and appropriateness of the test facility, test procedures, and low reduced frequency predictions.

The MCA airfoil pressure and suction surface data did not exhibit this same overall excellent correlation with prediction. The aerodynamic phase lag data exhibited a reasonable correlation with the predictions. However, the unsteady pressure coefficient correlation, while agreeing in trend with the prediction, only correlated well near the trailing edges of the surfaces.

References

[1] Chadwick, W. R., Bell, J. K., and Platzer, M. F., "On the Analysis of Supersonic Flow Past Oscillating Cascades," *Unsteady Phenomena in Turbomachinery*, AGARD Conference Proceedings No. 177, Sept. 1975.

[2] Kurosaka, M., "On the Flow Field of a Rapidly Oscillating Airfoil in a Supersonic Flow," *Journal of Fluid Mechanics*, Vol. 62, 1974.

[3] Kurosaka, M., "Cumulative Nonlinear Distortion of an Acoustic Wave Propagating through Nonuniform Flow," General Electric Company, Research and Development Center.

[4] Verdon, J. M., "The Unsteady Supersonic Flow Downstream of an Oscillating Airfoil," *Unsteady Flows in Jet Engines*, Office of Naval Research-Project SQUID Workshop, 1974.

[5] *Unsteady Phenomena in Turbomachinery*, AGARD Conference Proceedings No. 177, Sept. 1975.

[6] Fleeter, S. (ed), *Aeroelasticity in Turbomachines*, Office of Naval Research-Project SQUID Workshop, June 1972.

[7] Fleeter, S., Novick, A. S., and Riffel, R. E., "An Experimental Determination of the Unsteady Aerodynamics in a Controlled Oscillating Cascade," ASME Paper 76-GT-47, 1976.

[8] Miles, J. W., *The Potential Theory of Unsteady Supersonic Flow*, Chap. 13, Sec. 3, Cambridge University Press, 1959.